

Critical temperature of a Rashba spin-orbit-coupled Bose gas in a harmonic trap

Hui Hu and Xia-Ji Liu

ACQAO and Centre for Atom Optics and Ultrafast Spectroscopy, Swinburne University of Technology, Melbourne Victoria AU-3122, Australia

(Received 13 December 2011; published 12 January 2012)

We investigate theoretically Bose-Einstein condensation of an ideal, trapped Bose gas in the presence of Rashba spin-orbit coupling. Analytic results for the critical temperature and condensate fraction are derived based on a semiclassical approximation to the single-particle-energy spectrum and density of states and are compared with exact results obtained by explicitly summing discrete energy levels for a small number of particles. We find a significant decrease of the critical temperature and of the condensate fraction due to finite spin-orbit coupling. For a large coupling strength and a finite number of particles N , the critical temperature scales as $N^{2/5}$ and $N^{2/3}$ in three and two dimensions, respectively, contrasted to the predictions of $N^{1/3}$ and $N^{1/2}$ in the absence of spin-orbit coupling. Finite-size corrections in three dimensions are also discussed.

DOI: [10.1103/PhysRevA.85.013619](https://doi.org/10.1103/PhysRevA.85.013619)

PACS number(s): 67.85.-d, 05.30.Rt, 03.75.Kk, 03.75.Mn

I. INTRODUCTION

The recent experiment on spin-orbit-coupled spinor Bose gases of ^{87}Rb atoms [1] has stimulated great interest in the theoretical study of spin-orbit (SO) physics in both Bose-Einstein condensation (BEC) and fermionic superfluidity. It is well-known that the SO coupling leads to many interesting phenomena in condensed-matter physics. Typical examples are the recently discovered topological insulators (or quantum-spin Hall states) [2,3]. In degenerate atomic gases, due to unprecedented controllability in the interatomic interaction, geometry, and purity [4,5], SO coupling may bring about even more intriguing states of matter [6–24].

For a SO-coupled BEC, nontrivial structures, such as the density-stripe state [9,11], half-quantum vortex state [10], and lattice state [13,14], are predicted. For an atomic Fermi gas near Feshbach resonances, new two-fermion-bound states with anisotropic mass are formed even at a negative s -wave-scattering length [18,21,22], leading to the prospect of anisotropic superfluidity with mixed s - and p -wave components [22]. By imposing an external Zeeman field, novel topological superfluids supporting zero-energy Majorana modes may also emerge [20,23,24]. To observe these new states of matter, it is necessary to cool the temperature below a threshold, which may depend critically on the SO coupling. The purpose of this work is to determine the critical temperature of trapped atomic Bose gases with Rashba-type SO coupling. We focus on an ideal, noninteracting Bose gas since the critical temperature is less affected by weak interatomic interactions [25].

Theoretically, the critical temperature of a homogeneous Bose gas is greatly suppressed by the Rashba SO coupling as the low-energy density of states (DOS) is dramatically modified [6,18]. In three dimensions (3D) without Rashba SO coupling, the low-energy DOS $\rho(E)$ vanishes as \sqrt{E} . As a result, the number of total particles occupied at finite energy levels, given by $N(T) = \int_0^\infty dE \rho(E) / (e^{E/k_B T} - 1)$, saturates at the finite temperature T [4]. This leads to the well-known macroscopic occupation of the ground state, i.e., the formation of a BEC. In the presence of Rashba SO coupling, however, the low-energy DOS becomes a constant (see Appendix) [6,18], reminiscent of a two-dimensional (2D) system. The thermal occupation $N(T)$ can be logarithmically

divergent. The critical temperature is therefore precisely zero, ruling out the possibility of BEC at any finite temperatures [4].

In this paper, we show that in the presence of a harmonic trap the Rashba SO coupling does not destroy the BEC at finite temperatures as the thermal occupation $N(T)$ remains finite. Actually, the critical temperature is not affected by the Rashba SO coupling in the thermodynamic limit in which the number of particles N becomes infinitely large. This is because the occupation of low-energy states, modified by the SO coupling, becomes negligible as $N \rightarrow \infty$. However, in the experimentally relevant situation in which numbers of particles range from a few thousand to a few million, we find a significant decrease of the critical temperature and of the condensate fraction. In particular, at a sufficiently large Rashba SO-coupling strength, the critical temperature scales like $N^{2/5}$ and $N^{2/3}$ in three and two dimensions, respectively, in sharp contrast to the scaling of $N^{1/3}$ and $N^{1/2}$ without SO coupling [4,26–28]. We derive these results either by summing discrete energy levels for a small number of particles or by using a continuous DOS under the semiclassical assumption that the level spacing is negligible compared to the temperature. The former approach also enables an investigation of the finite-size correction to the critical temperature.

The paper is structured as follows. In the next section (Sec. II), we introduce the theoretical model for a Rashba spin-orbit-coupled ideal Bose gas in a harmonic trap and solve the single-particle-energy spectrum. In Sec. III, we present the 2D and 3D densities of states both with and without the continuous-spectrum approximation. The critical temperature and condensate fraction are then calculated in Sec. IV for both the 2D and 3D cases. Next, the finite-size effect in 3D is discussed in Sec. V. Finally, Sec. VI is devoted to our conclusions. The calculation of the DOS of a homogeneous 3D Rashba SO-coupled system is given in the Appendix.

II. MODEL HAMILTONIAN AND SINGLE-PARTICLE-ENERGY SPECTRUM

We consider a two-component (spin-1/2) Bose gas in both 2D and 3D harmonic traps, $V_{2D}(r_\perp) = M\omega_\perp^2(x^2 + y^2)/2 \equiv M\omega_\perp^2 r_\perp^2/2$ and $V_{3D}(r_\perp, z) = M(\omega_\perp^2 r_\perp^2 + \omega_z^2 z^2)/2$, respectively, with Rashba SO coupling $\mathcal{V}_{\text{SO}} = -i\lambda_R(\hat{\sigma}_x \partial_y - \hat{\sigma}_y \partial_x)$ in the xy plane, where λ_R is the Rashba SO-coupling

strength and $\hat{\sigma}_x$, $\hat{\sigma}_y$, and $\hat{\sigma}_z$ are the 2×2 Pauli matrices for pseudospin. The model Hamiltonian for a single particle is described by

$$\mathcal{H}_S = \begin{bmatrix} -\hbar^2 \nabla^2 / 2M + V_T & -i\lambda_R(\partial_y + i\partial_x) \\ -i\lambda_R(\partial_y - i\partial_x) & -\hbar^2 \nabla^2 / 2M + V_T \end{bmatrix}, \quad (1)$$

where the trapping potential $V_T(\mathbf{r}_\perp) = V_{2D}(r_\perp)$ in 2D and $V_T(\mathbf{r}) = V_{3D}(r_\perp, z)$ in 3D harmonic traps. The characteristic length scales of harmonic traps in the xy plane and z direction are given by $a_\perp = \sqrt{\hbar/(M\omega_\perp)}$ and $a_z = \sqrt{\hbar/(M\omega_z)}$, respectively. For the SO coupling, we take a dimensionless coupling strength $\lambda_{SO} \equiv \lambda_R M a_\perp / \hbar^2$.

In the 2D case, it is convenient to use polar coordinates $\mathbf{r}_\perp = (r_\perp, \varphi)$ in which $-i(\partial_y \pm i\partial_x) = e^{\mp i\varphi} [\pm \partial/\partial r_\perp - (i/r_\perp)\partial/\partial\varphi]$. As the harmonic potential is isotropic, the single-particle wave function has a well-defined azimuthal angular momentum $l_z = m$ and takes the form

$$\phi_m(\mathbf{r}_\perp) = \begin{bmatrix} \phi_\uparrow(r_\perp) \\ \phi_\downarrow(r_\perp)e^{i\varphi} \end{bmatrix} \frac{e^{im\varphi}}{\sqrt{2\pi}}, \quad (2)$$

which preserves the total angular momentum $j_z = l_z + s_z = m + 1/2$. The Schrödinger equation for $\phi_\uparrow(r_\perp)$ and $\phi_\downarrow(r_\perp)$ therefore becomes

$$\begin{bmatrix} \mathcal{H}_m & \lambda_R [\partial/\partial r_\perp + (m+1)/r_\perp] \\ \lambda_R (-\partial/\partial r_\perp + m/r_\perp) & \mathcal{H}_{m+1} \end{bmatrix} \times \begin{bmatrix} \phi_\uparrow \\ \phi_\downarrow \end{bmatrix} = E_{nm} \begin{bmatrix} \phi_\uparrow \\ \phi_\downarrow \end{bmatrix}, \quad (3)$$

where $\mathcal{H}_m \equiv -[\hbar^2/(2M)][d/dr_\perp^2 + (1/r_\perp)d/dr_\perp - m^2/r_\perp^2] + M\omega_\perp^2 r_\perp^2/2$ is the 2D harmonic oscillator. We have denoted the energy level as E_{nm} with $n = (0, 1, 2, \dots)$ being the good quantum number in the transverse (radial) direction. Each energy level is twofold degenerate as a result of the time-reversal symmetry satisfied by the single-particle model Hamiltonian (Kramers degeneracy). Any state $\phi(\mathbf{r}_\perp) = [\phi_\uparrow(\mathbf{r}_\perp), \phi_\downarrow(\mathbf{r}_\perp)]^T$ is degenerate with its time-reversal partner $\mathcal{T}\phi(\mathbf{r}_\perp) \equiv (i\sigma_y \mathcal{C})\phi(\mathbf{r}_\perp) = [\phi_\downarrow^*(\mathbf{r}_\perp), -\phi_\uparrow^*(\mathbf{r}_\perp)]^T$, where \mathcal{C} is the complex-conjugate operator. Therefore, we may restrict the quantum number m to non-negative integers as a state with negative m can always be treated as the time-reversal partner of a state with $m \geq 0$. To solve numerically the single-particle spectrum, we expand the wave function using the basis of a 2D harmonic oscillator

$$\phi_\uparrow(r_\perp) = \sum_{k=0}^{\infty} A_{\uparrow k} R_{km}(r_\perp), \quad (4)$$

$$\phi_\downarrow(r_\perp) = \sum_{k=0}^{\infty} A_{\downarrow k} R_{k, m+1}(r_\perp), \quad (5)$$

where

$$R_{km} = \frac{1}{a_\perp} \left[\frac{2k!}{(k+|m|)!} \right]^{1/2} \left(\frac{r_\perp}{a_\perp} \right)^{|m|} e^{-\frac{r_\perp^2}{2a_\perp^2}} \mathcal{L}_k^{|m|} \left(\frac{r_\perp^2}{a_\perp^2} \right) \quad (6)$$

is the radial wave function of \mathcal{H}_m with energy $(2k + |m| + 1)\hbar\omega_\perp$ and $\mathcal{L}_k^{|m|}$ is the associated Legendre polynomial. This leads to the following secular equation

$$\begin{bmatrix} \mathcal{H}_m & \mathcal{M}^T \\ \mathcal{M} & \mathcal{H}_{m+1} \end{bmatrix} \begin{bmatrix} A_\uparrow \\ A_\downarrow \end{bmatrix} = E_{nm} \begin{bmatrix} A_\uparrow \\ A_\downarrow \end{bmatrix}, \quad (7)$$

where the vectors A_\uparrow and A_\downarrow denote collectively the expanding coefficients $\{A_{\uparrow k}\}$ and $\{A_{\downarrow k}\}$, respectively, and the elements of the matrices ($m \geq 0$) are given by

$$(\mathcal{H}_m)_{kk'} = (2k + m + 1)\delta_{kk'}\hbar\omega_\perp, \quad (8)$$

$$\mathcal{M}_{kk'} = \lambda_{SO}(\sqrt{k' + m + 1}\delta_{kk'} + \sqrt{k'}\delta_{kk'-1})\hbar\omega_\perp. \quad (9)$$

Diagonalization of the secular matrix of Eq. (7) leads to the single-particle spectrum and single-particle wave functions. In numerical calculations, it is necessary to truncate the radial quantum number k of the 2D harmonic oscillator by restricting $k < k_{\max}$. For $\lambda_{SO} \leq 20$, we find that $k_{\max} = 256$ is already sufficiently large to have an accurate energy spectrum. With this cutoff, the dimension of the secular matrix in Eq. (7) is $2k_{\max} = 512$.

In Fig. 1(a), we present the single-particle-energy spectrum at $\lambda_{SO} = 5$. The ground-state single-particle energy is plotted in Fig. 1(b) as a function of the dimensionless SO-coupling constant. In reference to the semiclassical zero-point energy $E_0^{\text{sc}} \equiv -(\lambda_{SO}^2/2)\hbar\omega_\perp$, the ground-state energy decreases from $\hbar\omega_\perp$ to $\hbar\omega_\perp/2$ when the Rashba SO-coupling strength λ_{SO} becomes sufficiently large. In that limit (i.e., $\lambda_{SO} > 5$), the low-lying-energy spectrum becomes fairly flat with a dispersion that is well approximated by [13,14]

$$E_{nm} \simeq \left[-\frac{\lambda_{SO}^2}{2} + \left(n + \frac{1}{2}\right) + \frac{m(m+1)}{2\lambda_{SO}^2} \right] \hbar\omega_\perp. \quad (10)$$

In 3D, because the motions in the xy plane and the z direction are decoupled, the single-particle-energy spectrum is given by

$$E_{nmn_z} = E_{nm} + \left(n_z + \frac{1}{2}\right)\hbar\omega_z, \quad (11)$$

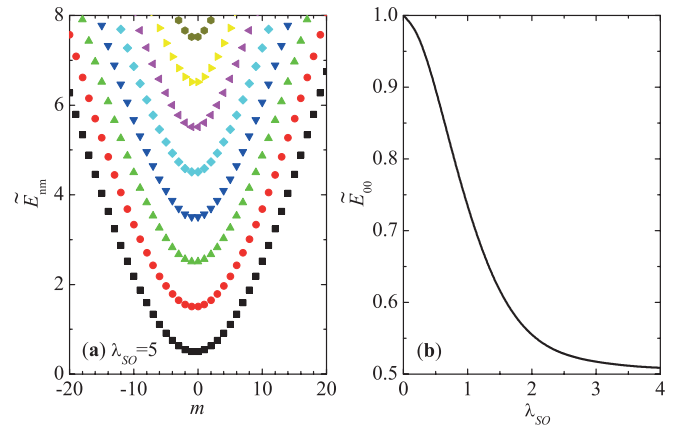


FIG. 1. (Color online) (a) Single-particle-energy spectrum $\tilde{E}_{nm} = E_{nm} + (\lambda_{SO}^2/2)\hbar\omega_\perp$ at $\lambda_{SO} = 5$, measured in reference to the semiclassical zero-point energy $-(\lambda_{SO}^2/2)\hbar\omega_\perp$. (b) Ground-state single-particle energy $\tilde{E}_{00} = E_{00} + (\lambda_{SO}^2/2)\hbar\omega_\perp$ as a function of the dimensionless Rashba SO-coupling constant. The energy is plotted in units of $\hbar\omega_\perp$.

where $n_z = 0, 1, 2, \dots$ is a good quantum number for the axial motion.

At finite temperature T , the total number of particles is given in the grand canonical ensembles by the sum

$$N = \sum_{n,m=0}^{\infty} \frac{2}{\exp[(E_{nm} - \mu)/k_B T] - 1} \quad (12)$$

in 2D and by the sum

$$N = \sum_{n,m,n_z=0}^{\infty} \frac{2}{\exp[(E_{nmn_z} - \mu)/k_B T] - 1} \quad (13)$$

in 3D, where μ is the chemical potential and the factor of 2 arises from the Kramers degeneracy. The sum can be rewritten as an integral over the energy in the unified form

$$N = \int_{-\infty}^{+\infty} dE \frac{\rho(E)}{\exp[(E - \mu)/k_B T] - 1} \quad (14)$$

with the DOS $\rho(E)$ given by

$$\rho_{2D}(E) = 2 \sum_{n,m=0}^{\infty} \delta(E - E_{nm}) \quad (15)$$

and

$$\rho_{3D}(E) = 2 \sum_{n,m,n_z=0}^{\infty} \delta(E - E_{nmn_z}) \quad (16)$$

in 2D and 3D, respectively.

For a given small number of particles N , we can calculate the low-lying-energy levels and then sum explicitly the number equations Eqs. (12) and (13). Once the chemical potential is determined at a given temperature T , we calculate the occupation of the ground state

$$N_0 = \frac{2}{\exp[(E_0 - \mu)/k_B T] - 1}, \quad (17)$$

where the single-particle ground-state energy $E_0 = E_{00}$ in 2D and $E_0 = E_{00} + \hbar\omega_z/2$ in 3D. The BEC transition temperature T_c can be determined from $d^2 N_0/dT^2$, exhibiting a maximum at T_c [29].

III. SEMICLASSICAL DENSITY OF STATES

For large numbers of particles, it is useful to consider a semiclassical approximation by using a continuous-energy spectrum [4]. The level spacing, typical of $\hbar\omega_{\perp}$ or $\hbar\omega_z$, is assumed to be negligibly small compared with the thermal energy $k_B T$. Thus, the relevant excitation energies, contributing to the sums in Eqs. (12) and (13), are much larger than the level spacing. The accuracy of the semiclassical approximation can be tested a posteriori by comparing the semiclassical result with the numerical discrete summation.

A. 2D density of states

In 2D, the semiclassical DOS can be written as

$$\rho_{2D}^{\text{sc}}(E) = \sum_{s=\pm} \int \frac{d\mathbf{r}_{\perp} d\mathbf{k}_{\perp}}{(2\pi)^2} \delta[E_{k_s}(\mathbf{r}_{\perp}) - E], \quad (18)$$

where $E_{k_s}(\mathbf{r}_{\perp}) = \hbar^2 k_{\perp}^2/(2M) + s\lambda_R k_{\perp} + M\omega_{\perp}^2 r_{\perp}^2/2$ is the semiclassical energy in the phase space $(\mathbf{r}_{\perp}, \mathbf{k}_{\perp})$. Because of the Rashba SO coupling, the semiclassical energy splits into two helicity branches as indicated by $s = \pm$ (see Appendix). By integrating out the spatial degree of freedom, we obtain that

$$\hbar\omega_{\perp} \rho_{2D}^{\text{sc}}(E) = \sum_{s=\pm} \int_0^{\infty} \tilde{k}_{\perp} d\tilde{k}_{\perp} \Theta \left[\frac{\tilde{E}}{\hbar\omega_{\perp}} - \frac{(\tilde{k}_{\perp} + s\lambda_{\text{SO}})^2}{2} \right], \quad (19)$$

where $\tilde{k}_{\perp} \equiv k_{\perp} a_{\perp}$ is the dimensionless wave vector, $\tilde{E} \equiv E + (\lambda_{\text{SO}}^2/2)\hbar\omega_{\perp}$ is the energy measured in reference to the semiclassical zero-point energy $E_0^{\text{sc}} \equiv -(\lambda_{\text{SO}}^2/2)\hbar\omega_{\perp}$, and $\Theta(\cdot)$ is the Heaviside step function. The integration over the wave vector can be calculated explicitly as well. We finally arrive at

$$\hbar\omega_{\perp} \rho_{2D}^{\text{sc}}(E) = \begin{cases} 0 & (E < E_0^{\text{sc}}), \\ 2\lambda_{\text{SO}} [2E/(\hbar\omega_{\perp}) + \lambda_{\text{SO}}^2]^{1/2} & (E_0^{\text{sc}} \leq E < 0), \\ 2E/(\hbar\omega_{\perp}) + 2\lambda_{\text{SO}}^2 & (E \geq 0). \end{cases} \quad (20)$$

In the absence of Rashba SO coupling ($\lambda_{\text{SO}} = 0$), we recover the usual expression for the 2D DOS in harmonic traps $\rho_{2D}^{\text{sc}}(E) = 2E/(\hbar\omega_{\perp})^2 \Theta(E)$ for a two-component system [4].

B. 3D density of states

Likewise, we calculate the semiclassical DOS in 3D, which is given by

$$\rho_{3D}^{\text{sc}}(E) = \sum_{s=\pm} \int \frac{d\mathbf{r} d\mathbf{k}}{(2\pi)^3} \delta[E_{k_s}(\mathbf{r}) - E], \quad (21)$$

where the semiclassical energy now takes the form $E_{k_s}(\mathbf{r}) = \hbar^2 k_{\perp}^2/(2M) + s\lambda_R k_{\perp} + \hbar^2 k_z^2/(2M) + M(\omega_{\perp}^2 r_{\perp}^2 + \omega_z^2 z^2)/2$. The integration over \mathbf{r} and k_z can be done by introducing a new variable $t^2 = \hbar^2 k_z^2/(2M) + M(\omega_{\perp}^2 r_{\perp}^2 + \omega_z^2 z^2)/2$ and by converting the variables of integration $d\mathbf{r} d\mathbf{k}$ to $dt d\mathbf{k}_{\perp}$. This leads to

$$\hbar\omega_z \rho_{3D}^{\text{sc}}(E) = \sum_{s=\pm} \int_0^{\infty} \tilde{k}_{\perp} d\tilde{k}_{\perp} \left[\frac{\tilde{E}}{\hbar\omega_{\perp}} - \frac{(\tilde{k}_{\perp} + s\lambda_{\text{SO}})^2}{2} \right] \times \Theta \left[\frac{\tilde{E}}{\hbar\omega_{\perp}} - \frac{(\tilde{k}_{\perp} + s\lambda_{\text{SO}})^2}{2} \right]. \quad (22)$$

By explicitly integrating out \tilde{k}_{\perp} , we obtain

$$\hbar\omega_z \rho_{3D}^{\text{sc}}(E) = \begin{cases} 0 & (E < E_0^{\text{sc}}), \\ (2\lambda_{\text{SO}}/3) [2E/(\hbar\omega_{\perp}) + \lambda_{\text{SO}}^2]^{3/2} & (E_0^{\text{sc}} \leq E < 0), \\ [E/(\hbar\omega_{\perp}) + \lambda_{\text{SO}}^2]^2 - \lambda_{\text{SO}}^4/3 & (E \geq 0). \end{cases} \quad (23)$$

In the absence of Rashba SO coupling, we recover the expression $\rho_{3D}^{\text{sc}}(E) = E^2/(\hbar^3 \omega_{\perp}^2 \omega_z) \Theta(E)$ for 3D harmonic traps [4].

It is easy to check that the 2D and 3D densities of states are related by

$$\hbar\omega_z \frac{d\rho_{3D}^{\text{sc}}(E)}{dE} = \rho_{2D}^{\text{sc}}(E). \quad (24)$$

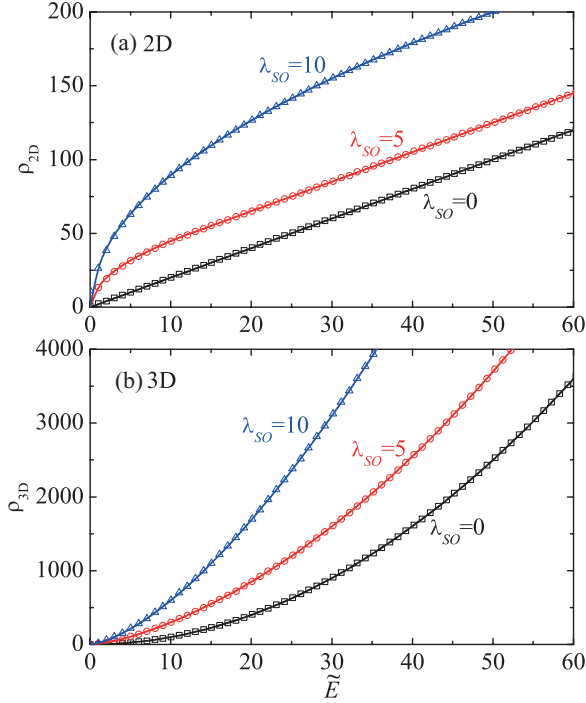


FIG. 2. (Color online) The semiclassical density of states in (a) 2D and (b) 3D in units of $1/(\hbar\omega_{\perp})$ and $1/(\hbar\omega_z)$, respectively, are shown as a function of $\tilde{E} = E + (\lambda_{SO}^2/2)\hbar\omega_{\perp}$ at different Rashba SO couplings (solid lines). The energy \tilde{E} is in units of $\hbar\omega_{\perp}$. For comparison, the symbols plot the results obtained by the numerical summation [see Eqs. (15) and (16)]. The simulation of the delta function is described in the text.

This is due to the decoupled motion in the xy plane and z direction, leading to the observation that the 3D energy spectrum may alternatively be viewed as a collection of 2D spectra with regular spacing $\hbar\omega_z$.

C. Test of the semiclassical DOS

In Fig. 2, we compare the semiclassical 2D and 3D densities of states with those obtained by summing over the discrete single-particle-energy spectrum using Eqs. (15) and (16). In the numerical summation, we simulate the δ function $\delta(x)$ by a Lorentzian line shape with broadening Γ , $f_{\delta}(x; \Gamma) = (\Gamma/\pi)/(x^2 + \Gamma^2)$. Roughly, the resulting DOS depends linearly on Γ as $\Gamma \sim \hbar\omega_{\perp}$. Therefore, we use

$$\delta(x) = 2f_{\delta}(x; \Gamma = \hbar\omega_{\perp}) - f_{\delta}(x; \Gamma = 2\hbar\omega_{\perp}) \quad (25)$$

as an extrapolation to the zero-broadening limit ($\Gamma = 0$). We find that the semiclassical expressions for the DOS [Eqs. (19) and (22)] work extremely well over a very broad range for energy. The most significant discrepancy occurs at the lowest energy level $E \sim -(\lambda_{SO}^2/2)\hbar\omega_{\perp}$ as anticipated.

IV. CRITICAL TEMPERATURE AND CONDENSATE FRACTION

We are now ready to calculate the critical temperature and condensate fraction for a large number of particles. With the

semiclassical DOS $\rho^{sc}(E)$, the number of particles could be rewritten as [4]

$$N = N_0 + \int_{E_0^{sc}}^{+\infty} dE \frac{\rho^{sc}(E)}{\exp[(E - \mu)/k_B T] - 1}, \quad (26)$$

where the ground-state population N_0 is singled out and the finite sums over the excited states in Eqs. (12) and (13) are replaced by an integral. Accordingly, we have set the lower bound of the integral to be the semiclassical zero-point energy $E_0^{sc} = -(\lambda_{SO}^2/2)\hbar\omega_{\perp}$. When BEC occurs, the chemical potential approaches E_0^{sc} from below [4]. The critical temperature T_c is determined by the condition

$$N = \int_0^{+\infty} d\tilde{E} \frac{\rho^{sc}(\tilde{E} + E_0^{sc})}{\exp(\tilde{E}/k_B T_c) - 1}, \quad (27)$$

where $\tilde{E} \equiv E - E_0^{sc}$, and the condensate fraction at $T < T_c$ can be calculated by

$$\frac{N_0}{N} = 1 - \frac{1}{N} \int_0^{+\infty} d\tilde{E} \frac{\rho^{sc}(\tilde{E} + E_0^{sc})}{\exp(\tilde{E}/k_B T) - 1}. \quad (28)$$

As we shall see, these equations can be conveniently solved by introducing $\epsilon = \tilde{E}/(k_B T)$ and

$$\alpha(T) = \lambda_{SO} \sqrt{\frac{\hbar\omega_{\perp}}{k_B T}}. \quad (29)$$

A. 2D

In 2D, the equations for the critical temperature and condensate fraction become

$$N = \left(\frac{k_B T_c}{\hbar\omega_{\perp}}\right)^2 \mathcal{I}_{2D}[\alpha(T_c)] \quad (30)$$

and

$$\frac{N_0}{N} = 1 - \left(\frac{T}{T_c}\right)^2 \frac{\mathcal{I}_{2D}[\alpha(T)]}{\mathcal{I}_{2D}[\alpha(T_c)]}, \quad (31)$$

respectively. Here the integral $\mathcal{I}_{2D}[\alpha]$ takes the form

$$\mathcal{I}_{2D}[\alpha] = \int_0^{+\infty} d\epsilon \frac{\tilde{\rho}_{2D}^{sc}(\epsilon; \alpha)}{e^{\epsilon} - 1}, \quad (32)$$

where the dimensionless DOS $\tilde{\rho}_{2D}^{sc}(\epsilon; \alpha)$ is given by

$$\tilde{\rho}_{2D}^{sc}(\epsilon; \alpha) = \begin{cases} 0 & (\epsilon < 0), \\ 2\alpha\sqrt{2\epsilon} & (0 \leq \epsilon < \alpha^2/2), \\ 2\epsilon + \alpha^2 & (\epsilon \geq \alpha^2/2). \end{cases} \quad (33)$$

Therefore,

$$\mathcal{I}_{2D}[\alpha] = \sqrt{2\pi}\alpha\zeta\left(\frac{3}{2}\right) + \int_{\alpha^2/2}^{+\infty} d\epsilon \frac{(\sqrt{2\epsilon} - \alpha)^2}{e^{\epsilon} - 1}. \quad (34)$$

Here $\zeta(\cdot)$ is the Riemann ζ function. $\mathcal{I}_{2D}[\alpha]$ depends implicitly on the temperature through the dimensionless parameter $\alpha(T)$. It is clear from Eq. (29) that for a given SO coupling λ_{SO} , the dimensionless parameter α at the critical temperature T_c always scales to zero in the thermodynamic limit $N \rightarrow \infty$. This is understandable as a finite SO interaction modifies only the low-lying-energy states, whose occupation becomes negligible as $N \rightarrow \infty$.

In the absence of SO coupling $\mathcal{I}_{2D}[\alpha = 0] = 2\zeta(2) = \pi^2/3$, we recover the standard results in 2D [4]:

$$k_B T_c^{(0)}(\lambda_{SO} = 0) = \frac{1}{\pi} (3N)^{1/2} \hbar \omega_{\perp} \quad (35)$$

and $N_0/N = 1 - (T/T_c^{(0)})^2$. Here, we use the superscript 0 to indicate the semiclassical result. For a large SO coupling $\mathcal{I}_{2D}[\alpha \gg 1] = \sqrt{2\pi\alpha}\zeta(3/2)$, we find that

$$k_B T_c^{(0)}(\lambda_{SO} \gg 1) = \frac{1}{(2\pi)^{1/3}} \left[\frac{N}{\lambda_{SO}\zeta(3/2)} \right]^{2/3} \hbar \omega_{\perp} \quad (36)$$

and $N_0/N = 1 - (T/T_c^{(0)})^{3/2}$. Thus, for a given number of particles, with increasing SO coupling the dependence of the 2D critical temperature on the number of particles changes from $N^{1/2}$ to $N^{2/3}$. Using $\alpha \gg 1$, the strong-coupling limit is reached when

$$\lambda_{SO} \gg (2\pi)^{-1/8} \left[\frac{N}{\zeta(3/2)} \right]^{1/4}. \quad (37)$$

In Fig. 3, we show $\mathcal{I}_{2D}[\alpha]$ as a function of the dimensionless parameter α . Empirically, we find that $\mathcal{I}_{2D}[\alpha] \simeq \sqrt{2\pi\alpha}\zeta(3/2) + 2\zeta(2)e^{-1.84\alpha - 0.13\alpha^2}$ within a 0.5% relative error. Figure 4 reports the critical temperature as a function of SO coupling for several different numbers of particles (solid lines). It decreases significantly at a moderate SO coupling ($\lambda_{SO} \sim 10$) and number of particles (i.e., $N \sim 10^4$). The strong-coupling results [Eq. (36)] have also been plotted using dot-dashed lines. Finally, in Fig. 5, we present the condensate fraction at $\lambda_{SO} = 5$ and $N = 10^3, 10^5$, and ∞ .

B. 3D

In 3D, similarly we obtain that

$$N\lambda = \left(\frac{k_B T_c}{\hbar \omega_{\perp}} \right)^3 \mathcal{I}_{3D}[\alpha(T_c)] \quad (38)$$

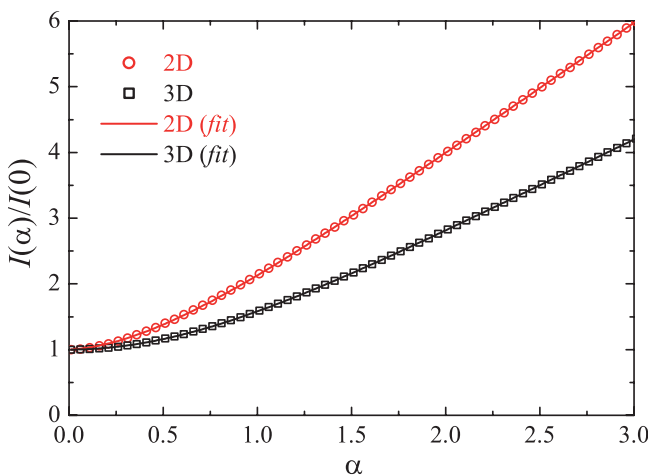


FIG. 3. (Color online) The integrals \mathcal{I}_{2D} and \mathcal{I}_{3D} as a function of the dimensionless parameter $\alpha = \lambda_{SO}[\hbar\omega_{\perp}/(k_B T)]^{1/2}$ (symbols). The solid lines show the empirical fit which agrees numerically within the 0.5% relative error (see the text for the empirical formalism).

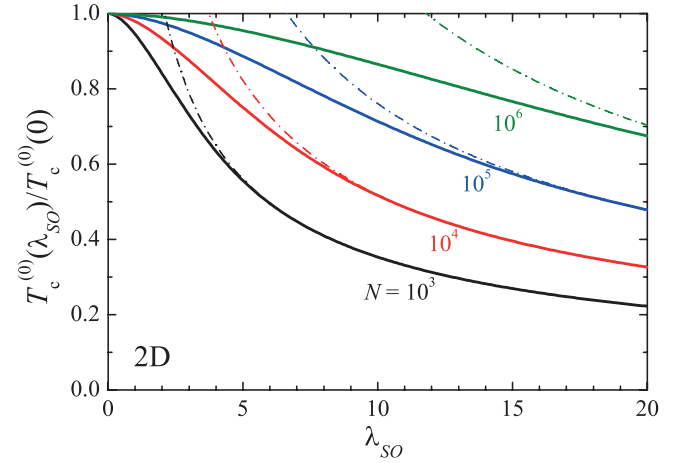


FIG. 4. (Color online) 2D critical temperature as a function of the SO coupling at different numbers of particles as indicated. The dot-dashed lines show the limiting behavior at large SO coupling [Eq. (36)].

and

$$\frac{N_0}{N} = 1 - \left(\frac{T}{T_c} \right)^3 \frac{\mathcal{I}_{3D}[\alpha(T)]}{\mathcal{I}_{3D}[\alpha(T_c)]}, \quad (39)$$

where $\lambda = \omega_z/\omega_{\perp}$ is the aspect ratio of the harmonic trap, the integral $\mathcal{I}_{3D}[\alpha]$ is given by

$$\mathcal{I}_{3D}[\alpha] = \int_0^{+\infty} d\epsilon \frac{\tilde{\rho}_{3D}^{sc}(\epsilon; \alpha)}{e^{\epsilon} - 1}, \quad (40)$$

and the dimensionless DOS $\tilde{\rho}_{3D}^{sc}(\epsilon; \alpha)$ is

$$\tilde{\rho}_{3D}^{sc}(\epsilon; \alpha) = \begin{cases} 0 & (\epsilon < 0), \\ (4\sqrt{2}\alpha/3)\epsilon^{3/2} & (0 \leq \epsilon < \alpha^2/2), \\ \epsilon^2 + \epsilon\alpha^2 - \alpha^4/12 & (\epsilon \geq \alpha^2/2). \end{cases} \quad (41)$$

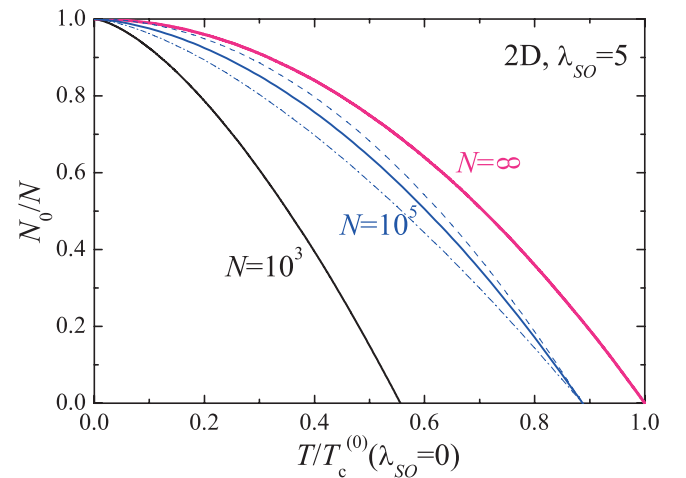


FIG. 5. (Color online) 2D condensate fraction at $\lambda_{SO} = 5$ and for different numbers of particles. For the case of $N = 10^5$, the dashed and dot-dashed lines show, respectively, the strong-coupling and zero-coupling results, $N_0/N = 1 - (T/T_c^{(0)})^2$ and $N_0/N = 1 - (T/T_c^{(0)})^{3/2}$.

Explicitly, we find that

$$\mathcal{I}_{3D}[\alpha] = \sqrt{2\pi}\alpha\zeta\left(\frac{5}{2}\right) + \int_{\alpha^2/2}^{+\infty} d\epsilon \frac{h(\epsilon)}{e^\epsilon - 1}, \quad (42)$$

where $h(\epsilon) = \epsilon^2 + \epsilon\alpha^2 - \alpha^4/12 - (4\sqrt{2}\alpha/3)\epsilon^{3/2}$. We plot $\mathcal{I}_{3D}[\alpha]$ in Fig. 3 together with an empirical fit $\mathcal{I}_{3D}[\alpha] = \sqrt{2\pi}\alpha\zeta(5/2) + 2\zeta(3)e^{-1.40\alpha - 0.30\alpha^2}$.

At $\lambda_{SO} = 0$ where $\mathcal{I}_{3D}[\alpha = 0] = 2\zeta(3)$, we obtain

$$k_B T_c^{(0)}(\lambda_{SO} = 0) = \left[\frac{N\lambda}{2\zeta(3)} \right]^{1/3} \hbar\omega_\perp \quad (43)$$

and $N_0/N = 1 - (T/T_c^{(0)})^3$, recovering the well-known 3D result for a trapped spin-1/2 Bose gas [4]. In the limit of large SO coupling in which $\mathcal{I}_{3D}[\alpha \gg 1] = \sqrt{2\pi}\alpha\zeta(5/2)$, we find instead

$$k_B T_c^{(0)}(\lambda_{SO} \gg 1) = \frac{1}{(2\pi)^{1/5}} \left[\frac{N\lambda}{\lambda_{SO}\zeta(5/2)} \right]^{2/5} \hbar\omega_\perp \quad (44)$$

and $N_0/N = 1 - (T/T_c^{(0)})^{5/2}$. Thus, for a given N with increasing SO coupling, the power-law dependence of the 3D critical temperature on the number of particles changes from $N^{1/3}$ to $N^{2/5}$. We estimate that the strong-coupling result is applicable if

$$\lambda_{SO} \gg (2\pi)^{-1/12} \left[\frac{N\lambda}{\zeta(5/2)} \right]^{1/6}. \quad (45)$$

In Fig. 6, we report the effect of the SO coupling on the 3D critical temperature. To make a connection with the National Institute of Standards and Technology experiment [1], we have used a realistic aspect ratio of the trapping potential and number of particles, $\lambda = \sqrt{8}$ and $N = 1.8 \times 10^5$. We also consider the case with a small number of particles $N = 10^3$. At the typical SO-coupling strength $\lambda_{SO} \sim 10$ [1], the reduction of the critical temperature is about 20%, which is in reach of current experiments. The inset shows the condensate fraction at $\lambda_{SO} = 5$.

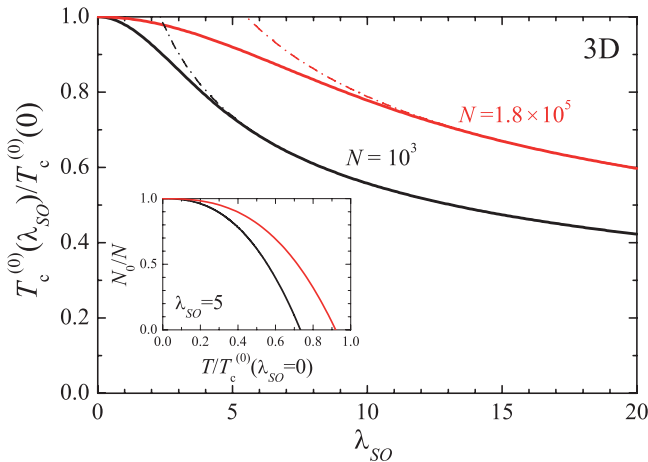


FIG. 6. (Color online) 3D critical temperature as a function of the SO-coupling strength at $N = 10^3$ and $N = 1.8 \times 10^5$. The aspect ratio of the harmonic trap is $\lambda = \omega_z/\omega_\perp = \sqrt{8}$. The dot-dashed lines show the critical temperature in the strong-coupling limit [Eq. (44)]. The inset reports the condensate fraction at $\lambda_{SO} = 5$.

V. FINITE-SIZE CORRECTION TO T_c IN 3D

We now turn to consider the finite-size correction to the semiclassical results, arising from the discreteness of the single-particle-energy spectrum [26,27]. The semiclassical results are obtained using the semiclassical approximation for the excited states and setting the chemical potential to the semiclassical zero-point energy E_0^{sc} . To the leading order, the finite-size correction can be included by still employing the semiclassical description for the excited states while keeping the quantum value $\mu = E_0$ for the chemical potential at the transition [25]. Here, $E_0 > E_0^{\text{sc}}$ is the single-particle energy of the ground state. It is E_{00} in 2D and $E_{00} + \hbar\omega_z/2$ in 3D [see, for example, Fig. 1(b) for E_{00} as a function of the SO-coupling strength]. The discreteness of the excited-energy spectrum gives rise to higher-order finite-size corrections. In the following, we focus on the finite-size correction to the 3D critical temperature.

Using the quantum value $\mu = E_0$ for the chemical potential, the 3D critical temperature is determined by

$$\begin{aligned} N &= \int_{E_0}^{+\infty} dE \frac{\rho_{3D}^{\text{sc}}(E)}{\exp[(E - E_0)/k_B T_c] - 1} \\ &= \int_0^{+\infty} dE \frac{\rho_{3D}^{\text{sc}}(\tilde{E} + E_0^{\text{sc}} + \Delta E)}{\exp(\tilde{E}/k_B T_c) - 1}, \end{aligned} \quad (46)$$

where in the second line we have introduced $\tilde{E} = E - E_0$ and $\Delta E = E_0 - E_0^{\text{sc}} > 0$. Compared with Eq. (27), the 3D DOS is slightly up-shifted by the amount ΔE . As $\Delta E \sim \hbar\omega_\perp$ is the smallest energy scale, using Eq. (24), we may write $\rho_{3D}^{\text{sc}}(\tilde{E} + E_0^{\text{sc}} + \Delta E) \simeq \rho_{3D}^{\text{sc}}(\tilde{E} + E_0^{\text{sc}}) + (\Delta E/\hbar\omega_z)\rho_{2D}^{\text{sc}}(\tilde{E} + E_0^{\text{sc}})$. Therefore, using the integrals \mathcal{I}_{2D} and \mathcal{I}_{3D} , the equation for the critical temperature is given by

$$N\lambda = \left(\frac{k_B T_c}{\hbar\omega_\perp} \right)^3 \left\{ \mathcal{I}_{3D}[\alpha(T_c)] + \frac{\Delta E}{k_B T_c} \mathcal{I}_{2D}[\alpha(T_c)] \right\}. \quad (47)$$

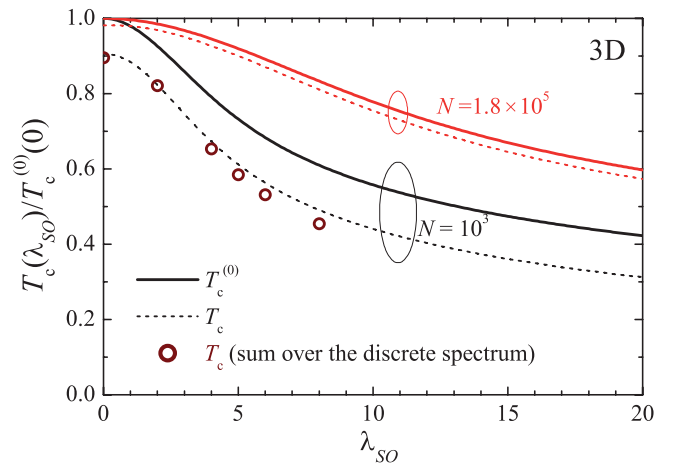


FIG. 7. (Color online) 3D transition temperature as a function of the SO coupling. The solid lines show the semiclassical predictions, and the dashed line gives the results with inclusion of the leading finite-size correction. The empty circles are calculated using the numerical summation for N_0 with the discrete energy spectrum, i.e., Eq. (17). The critical temperature is then determined from the peak position of $d^2 N_0/dT^2$ [29].

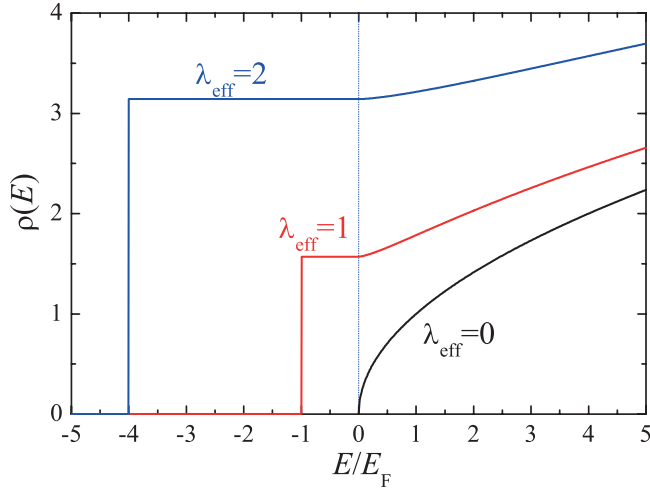


FIG. 8. (Color online) Density of states of a 3D homogeneous SO-coupled system at several SO-coupling strengths. The density of states is plotted in units of Mk_F/\hbar^2 .

In the absence of the SO coupling where $\mathcal{I}_{2D} = 2\zeta(2)$, $\mathcal{I}_{3D} = 2\zeta(3)$, and $\Delta E = \hbar\omega_\perp + \hbar\omega_z/2$, it is easy to verify that the transition temperature T_c is given by the law

$$\frac{T_c}{T_c^0} \simeq 1 - \frac{\zeta(2)}{[2\zeta(3)]^{2/3}} N^{-1/3} \frac{(2\hbar\omega_\perp + \hbar\omega_z)/3}{(\omega_\perp^2 \omega_z)^{1/3}}, \quad (48)$$

which is known in the literature [25–27].

In Fig. 7, we report the 3D transition temperature with the leading finite-size correction as shown by dashed lines. We find a sizable correction with a small number of particles (i.e., $N = 10^3$). For an experimentally realistic number of particles, i.e., $N = 1.8 \times 10^5$, however, the correction becomes mild. As a benchmark for our analytic treatment of T_c , we also show by

symbols the critical temperature for a small number of particles calculated by the discrete sum for the ground-state population N_0 [Eq. (17)]. For relatively small SO coupling (i.e., $\lambda_{SO} < 5$), our analytic treatment works very well. However, for large SO coupling, the single-particle level splitting between the ground state and the first excited state becomes increasingly small. We then may have to take into account the discreteness of the low-lying excited-energy levels.

VI. CONCLUSIONS

In summary, we have investigated the critical temperature and condensate fraction of a harmonically trapped ideal Bose gas in the presence of Rashba spin-orbit coupling by using either the exact numerical summation for a small number of particles or the analytic semiclassical approach for a large number of particles. The leading finite-size correction to the semiclassical approximation has also been considered. We have found a pronounced effect of the Rashba SO coupling. For the experimentally realistic number of particles ($N \sim 10^5$) [1], the critical temperature is reduced by more than 20% in magnitude at moderate SO coupling. This reduction is readily observable in current experiments. Moreover, in the limit of strong SO coupling, the critical temperature scales as $N^{2/5}$ and $N^{2/3}$ in three and two dimensions, respectively, which should be contrasted with the scaling law of $N^{1/3}$ and $N^{1/2}$ in the absence of SO coupling. Our investigation of critical temperature can be easily extended to include a weak repulsive interaction by using mean-field Hartree-Fock theory [25].

ACKNOWLEDGMENTS

This work was supported by the ARC Discovery Project (Grants No. DP0984522 and No. DP0984637) and NFRP-China (Grant No. 2011CB921502).

APPENDIX: DENSITY OF STATES OF A 3D HOMOGENEOUS SO-COUPLED SYSTEM

In free space, the single-particle Hamiltonian with Rashba SO coupling

$$\mathcal{H}_S = \begin{bmatrix} -\hbar^2 \nabla^2 / 2M & -i\lambda_R (\partial_y + i\partial_x) \\ -i\lambda_R (\partial_y - i\partial_x) & -\hbar^2 \nabla^2 / 2M \end{bmatrix} \quad (A1)$$

has the dispersion

$$E_{ks} = \frac{\hbar^2 k_z^2}{2M} + \frac{\hbar^2 k_\perp^2}{2M} + s\lambda_R k_\perp. \quad (A2)$$

Here $s = \pm$ denotes the two helicity branches. The DOS, given by $\rho(E) = (1/V) \sum_k [\delta(E_{k+} - E) + \delta(E_{k-} - E)]$, can be calculated analytically. We find that

$$\rho(E) = \frac{M^2 \lambda_R}{\hbar^4} \begin{cases} 0 & (E < -E_R/2), \\ \pi/2 & (-E_R/2 \leq E < 0), \\ \sqrt{2E/E_R} + (\pi/2 - \arctan \sqrt{2E/E_R}) & (E \geq 0), \end{cases} \quad (A3)$$

where $E_R \equiv M\lambda_R^2/\hbar^2$ is the characteristic energy related to the SO coupling. This result was reported by Hui Zhai in Ref. [6] [see for example, their Fig. 2(b)]. By introducing a Fermi wave vector $k_F = (3\pi^2 N/V)^{1/3}$, Fermi energy $E_F = \hbar^2 k_F^2/(2M)$, and dimensionless SO-coupling strength $\lambda_{\text{eff}} = M^2\lambda_R/(\hbar^2 k_F)$, the DOS can be written as

$$\rho(E) = \frac{Mk_F}{\hbar^2} \begin{cases} 0 & (E < -\lambda_{\text{eff}}^2), \\ \lambda_{\text{eff}}\pi/2 & (-\lambda_{\text{eff}}^2 \leq E < 0), \\ \sqrt{E/E_F} + \lambda_{\text{eff}}[\pi/2 - \arctan\sqrt{E/(\lambda_{\text{eff}}^2 E_F)}] & (E \geq 0). \end{cases} \quad (\text{A4})$$

We show in Fig. 8 the DOS at different SO-coupling strengths.

-
- [1] Y.-J. Lin, K. Jiménez-García, and I. B. Spielman, *Nature (London)* **471**, 83 (2011).
[2] X. L. Qi and S. C. Zhang, *Phys. Today* **63**, 33 (2010).
[3] M. Z. Hasan and C. L. Kane, *Rev. Mod. Phys.* **82**, 3045 (2010).
[4] F. Dalfvo, S. Giorgini, L. P. Pitaevskii, and S. Stringari, *Rev. Mod. Phys.* **71**, 463 (1999).
[5] I. Bloch, J. Dalibard, and W. Zwerger, *Rev. Mod. Phys.* **80**, 885 (2008).
[6] For a mini-review, see H. Zhai, e-print [arXiv:1110.6798](https://arxiv.org/abs/1110.6798).
[7] T. D. Stanescu, B. Anderson, and V. Galitski, *Phys. Rev. A* **78**, 023616 (2008).
[8] J. Larson and E. Sjöqvist, *Phys. Rev. A* **79**, 043627 (2009).
[9] C. Wang, C. Gao, C. M. Jian, and H. Zhai, *Phys. Rev. Lett.* **105**, 160403 (2010).
[10] C. Wu, I. Mondragon-Shem, and X.-F. Zhou, *Chin. Phys. Lett.* **28**, 097102 (2011).
[11] T.-L. Ho and S. Zhang, *Phys. Rev. Lett.* **107**, 150403 (2011).
[12] X. Q. Xu and J. H. Han, *Phys. Rev. Lett.* **107**, 200401 (2011).
[13] H. Hu, B. Ramachandran, H. Pu, and X.-J. Liu, *Phys. Rev. Lett.* **108**, 010402 (2012).
[14] S. Sinha, R. Nath, and L. Santos, *Phys. Rev. Lett.* **107**, 270401 (2011).
[15] R. Barnett, S. Powell, T. Gra, M. Lewenstein, and S. Das Sarma, e-print [arXiv:1109.4945](https://arxiv.org/abs/1109.4945).
[16] Q. Zhu, C. Zhang, and B. Wu, e-print [arXiv:1109.5811](https://arxiv.org/abs/1109.5811).
[17] Y. Deng, J. Cheng, H. Jing, C.-P. Sun, and S. Yi, e-print [arXiv:1110.0558](https://arxiv.org/abs/1110.0558).
[18] J. P. Vyasanakere and V. B. Shenoy, *Phys. Rev. B* **83**, 094515 (2011).
[19] M. Iskin and A. L. Subasi, *Phys. Rev. Lett.* **107**, 050402 (2011).
[20] S. L. Zhu, L. B. Shao, Z. D. Wang, and L. M. Duan, *Phys. Rev. Lett.* **106**, 100404 (2011).
[21] Z. Q. Yu and H. Zhai, *Phys. Rev. Lett.* **107**, 195305 (2011).
[22] H. Hu, L. Jiang, X.-J. Liu, and H. Pu, *Phys. Rev. Lett.* **107**, 195304 (2011).
[23] M. Gong, S. Tewari, and C. Zhang, *Phys. Rev. Lett.* **107**, 195303 (2011).
[24] X.-J. Liu, L. Jiang, H. Pu, and H. Hu, e-print [arXiv:1111.1798](https://arxiv.org/abs/1111.1798).
[25] S. Giorgini, L. P. Pitaevskii, and S. Stringari, *Phys. Rev. A* **54**, R4633 (1996).
[26] W. Ketterle and N. J. van Druten, *Phys. Rev. A* **54**, 656 (1996).
[27] H. Haugerud, T. Haugset, and F. Ravndal, *Phys. Lett. A* **225**, 18 (1997).
[28] A. Balaž, I. Vidanović, A. Bogojević, and A. Pelster, *Phys. Lett. A* **374**, 1539 (2010).
[29] T. Bergeman, D. L. Feder, N. L. Balazs, and B. I. Schneider, *Phys. Rev. A* **61**, 063605 (2000).